THz intersubband absorption in n-type Si$_{1-x}$Ge$_x$ parabolic quantum wells ⓔⓟ

ⓘⒹ Michele Montanari, Chiara Ciano, ⓘⒹ Luca Persichetti, et al.

COLLECTIONS

ⒺⓅ This paper was selected as an Editor's Pick

View Online   Export Citation   CrossMark

ARTICLES YOU MAY BE INTERESTED IN

THz intersubband electroluminescence from n-type Ge/SiGe quantum cascade structures
Applied Physics Letters **118**, 101101 (2021); https://doi.org/10.1063/5.0041327

Monolithic infrared silicon photonics: The rise of (Si)GeSn semiconductors
Applied Physics Letters **118**, 110502 (2021); https://doi.org/10.1063/5.0043511

Polarization switching in Bi$_{0.8}$La$_{0.2}$FeO$_3$ films with ferroelectric/semiconductor heterojunctions
Applied Physics Letters **118**, 162904 (2021); https://doi.org/10.1063/5.0039567
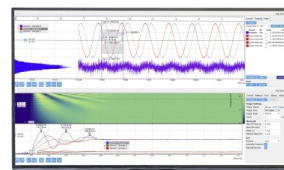
THz intersubband absorption in n-type Si$_{1-x}$Ge$_x$ parabolic quantum wells (EP)

View Online   Export Citation   CrossMark

Michele Montanari,[1,a)] (iD) Chiara Ciano,[1] Luca Persichetti,[1] (iD) Cedric Corley,[2] Leonetta Baldassarre,[3] (iD)
Michele Ortolani,[3] (iD) Luciana Di Gaspare,[1] (iD) Giovanni Capellini,[1,2] (iD) David Stark,[4] (iD)
Giacomo Scalari,[4] (iD) Michele Virgilio,[5] (iD) and Monica De Seta[1,b)] (iD)

AFFILIATIONS

[1]Dipartimento di Scienze, Università degli Studi Roma Tre, V.le G. Marconi 446, 00146 Rome, Italy
[2]IHP-Leibniz-Institut für Innovative Mikroelektronik, Im Technologiepark 25, 15236 Frankfurt (Oder), Germany
[3]Dipartimento di Fisica, Università di Roma "Sapienza," Piazzale A. Moro 2, 00185 Rome, Italy
[4]Institute for Quantum Electronics, Department of Physics, ETH Zürich, Wolfgang-Pauli-Strasse 16, 8093 Zürich, Switzerland
[5]Dipartimento di Fisica "E. Fermi," Università di Pisa, Largo Pontecorvo 3, 56127 Pisa, Italy

a)Present address: Dipartimento di Fisica e Astronomia, Università degli Studi di Firenze, Via G. Sansone 1, 50019 Sesto Fiorentino,
Italy. **Author to whom correspondence should be addressed:** montanari@lens.unifi.it
b)Electronic mail: monica.deseta@uniroma3.it

ABSTRACT

High-quality n-type continuously graded Ge-rich Si$_{1-x}$Ge$_x$ parabolic quantum wells with different doping levels were grown by using ultrahigh-vacuum chemical vapor deposition on Si(001) substrates. A thorough structural characterization study highlights an ideal parabolic compositional profile. THz intersubband absorption has been investigated in modulation-doped samples and samples directly doped in the wells. The comparison of experimental absorption data and theoretical calculations allowed us to quantify the impact of electron correlation effects on the absorption resonances in the different doping conditions and for electron sheet densities in the $(1 \div 6) \times 10^{11}$ cm^{-2} range. A single optical resonance is present in modulation doped samples. Its peak energy and line shape are independent of temperature-induced variations of the electron distribution in the subbands up to 300 K, in agreement with the generalized Kohn theorem. This achievement represents a relevant step forward for the development of CMOS compatible optoelectronic devices in the THz spectral range, where thermal charge fluctuations play a key role.

Published under license by AIP Publishing. https://doi.org/10.1063/5.0048344

Intersubband transitions (ISBTs) in semiconductor quantum wells (QWs) have been the focus of intense research in the last few decades due to their importance for optoelectronic devices, such as quantum cascade lasers[1–3] and quantum well photodetectors,[4,5] and the rich physics that can be investigated, like the strong and ultrastrong light-matter coupling.[6–8] In this context, parabolic quantum wells (PQWs) have been recently identified as a particularly interesting quantum system.[9–11] The main key feature of ISBTs in PQWs is that, according to the generalized Kohn theorem,[12,13] their energy is independent of the density and distribution of electrons in the QW. This is extremely relevant in THz optoelectronics where thermal charge fluctuations play a key role. PQWs have been proposed[9] as promising candidates for the development of THz sources operating at room temperature, with relevant applications in several fields, ranging from biology, medicine, and security communications.[14] Furthermore, the use of PQWs in optical

microcavities allowed observation of strong light matter coupling at room temperature, where the thermal energy kT is larger than the photon energy,[15] and to reach the ultrastrong coupling regime.[10]

Most of the PQW structures investigated so far have been realized in III–V material systems[9,11,15–19] by exploiting molecular beam epitaxy (MBE). Despite the fact that the growth of III–V rectangular QWs by MBE is very well developed, the deposition of high-quality graded PQWs has been shown to be more challenging. Hence, many works[9,15–17] exploited the digital alloy growth technique, which consists in alternating layers of different compositions to create an effective parabolic potential for the carriers. As a main drawback, the resulting structure shows a large number of interfaces, which are the source of undesirable scattering.

Recently, n-type Ge/SiGe heterostructures characterized by L-valley electrons having an effective mass of $m_z^* = 0.135\,m_0$[20] have
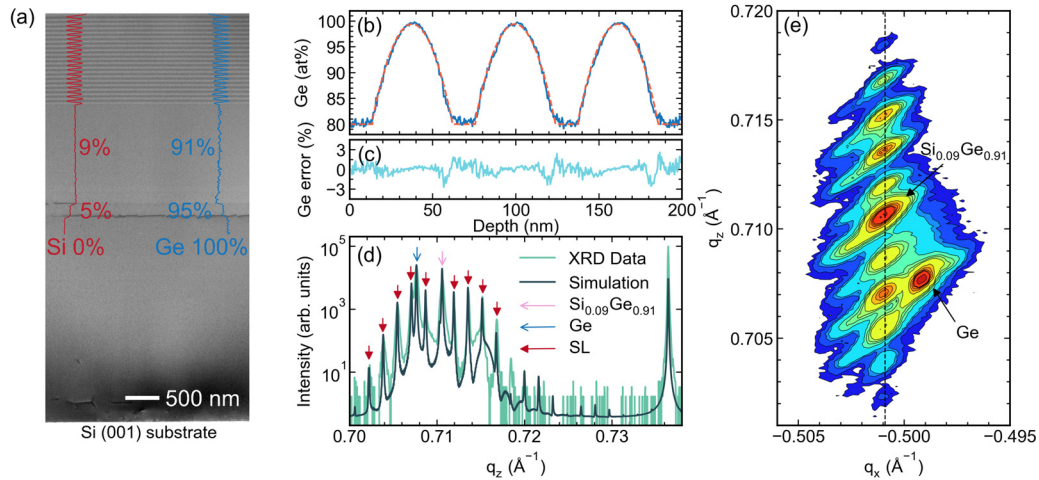
FIG. 1. (a) SIMS composition profile of a PQW sample superimposed on its STEM image. (b) Enlarged view of the SIMS composition profile (blue curve) and parabolic fit (orange curve). Panel (c) shows the difference between the two curves in (b). (d) (004) XRD rocking curve and (e) reciprocal space map of asymmetric (4$\bar{2}\bar{2}$) reflections.

been indicated as promising candidates for realizing room temperature CMOS-compatible THz emitters, which are more appealing for industrial applications. However, in the deposition of Ge-rich SiGe heterostructures on Si substrates, additional complexity arises from the 4.2% lattice mismatch between Ge and Si.[21] Furthermore, the achievement of a parabolic compositional profile is also complicated by surface segregation of Ge and Si–Ge intermixing occurring during the growth.[22]

In this Letter, we demonstrate the deposition of a stack of identical n-doped, continuously graded Ge-rich $Si_{1-x}Ge_x$ PQWs. By exploring samples with different doping levels and doping geometry, we investigate ISB absorption spectra as a function of temperature, within the range from 10 K up to 300 K. Supported by theoretical calculations, we experimentally verify that in modulation doped samples, electron–electron interactions cancel out; thus, the absorption resonance is entirely governed by the bare parabolic potential, and it is independent of the electron distribution in the subbands and of temperature, also for high doping levels. Furthermore, we establish the maximum doping level for which electron correlation effects are negligible and the absorption spectral line shape is independent of temperature also in samples directly doped in the wells.

The PQW samples have been grown by ultrahigh-vacuum chemical vapor deposition (UHV-CVD) on Si(001) substrates by using ultrapure silane (SiH_4) and germane (GeH_4) without carrier gas. To achieve SiGe layers with a high Ge concentration and low threading dislocation densities (TDD $\sim 3.5 \times 10^6$ cm^{-2}), the PQWs have been deposited on top of an SiGe reverse-graded virtual substrate (VS),[23] with a final $Si_{0.09}Ge_{0.91}$ alloy layer [see Fig. 1(a)], which ensures the strain-balance condition in the QW region, preventing its plastic relaxation. The parabolic $Si_{1-x}Ge_x$ compositional profile, with x in the range of 0.8–1, is obtained by keeping the GeH_4 gas flow constant and continuously varying the SiH_4 flow by means of calibrated mass flow controllers. The module composed by the parabolic well and a $Si_{0.20}Ge_{0.80}$ barrier has been repeated 20 times. To populate the fundamental subband, the samples were n-doped by using phosphine co-deposition in the central 5 nm of the parabolic well (direct doping, samples D-LD and D-HD) or in the central 5 nm of the 13 nm thick

$Si_{0.20}Ge_{0.80}$ barrier (modulation doping, sample M-HD), leaving an undoped $Si_{0.20}Ge_{0.80}$ layer between the dopants and the well to reduce ionized impurity scattering.[24] The nominal donor densities N_{3D} are about 4×10^{17} cm^{-3} and 1×10^{18} cm^{-3} for low and high doping samples, respectively, as estimated on the basis of secondary ion mass spectrometry (SIMS) measurements performed on thick Ge and SiGe calibration samples. Due to the possible inaccuracy when using such a calibration procedure for the very thin doped region here used, the actual sheet-carrier density n_{2D} of each sample was directly measured from the Fourier Transform Infrared (FTIR) absorption spectra, following the procedure reported in Ref. 35. The samples were characterized by using high resolution x-ray diffraction (HR-XRD), SIMS, scanning transmission electron microscopy (STEM), and FTIR spectroscopy. Specific information on individual samples can be found in Table I.

Figure 1(a) shows the SIMS composition profile of a PQW sample superimposed on the corresponding STEM image. Between the thick $Si_{0.09}Ge_{0.91}$ alloy and the Ge layer, we clearly observe the interfaces corresponding to the thin $Si_{0.05}Ge_{0.95}$ layer, where the STEM contrast is due to the presence of misfit dislocations. No threading dislocations are observed within the field of view of the STEM image in accordance with the TDD count of $\sim 3.5 \times 10^6$ cm^{-2}. The compositional profile across the PQWs has been accurately evaluated by SIMS. The results reported in Figs. 1(b) and 1(c) show that the profile of the Ge composition accurately matches a parabola. The small

TABLE I. Sample parameters. The labeling is defined as M (D) for modulation (direct) doping—HD (LD) for high (low) doping. The sheet-carrier density n_{2D} is estimated from FTIR absorption spectra following the procedure reported in Ref. 35.

| Sample	Doping geometry	n_{2D} (cm^{-2})
D-LD	Direct	1.5×10^{11}
M-HD	Modulation	3.5×10^{11}
D-HD	Direct	6.0×10^{11}

discrepancy < 2.5% present in the region where the Ge content increases during the growth can be attributed to Ge segregation. We verified that this discrepancy affects the ISBT energies by less than 2%.

HR-XRD measurements, carried out using a Rigaku SmartLab diffractometer, are shown in Figs. 1(d) and 1(e). The positions of the VS spots associated with the Ge and the $Si_{0.09}Ge_{0.91}$ layers in the HR-XRD reciprocal space map around asymmetric $(4\bar{2}\bar{2})$ reflections reported in Fig. 1(e) reveal, at room temperature, a tensile strain of about +0.2%, which can be ascribed to the difference between the coefficients of thermal expansion in Ge and Si.[25,26] Together with the reflections due to the Ge and the $Si_{0.09}Ge_{0.91}$ layers, we observe multiple orders of superlattice (SL) satellites, resulting from the PQW periodicity, which are perfectly vertically aligned to the $Si_{0.09}Ge_{0.91}$ spot, indicating that the entire PQW stack is coherent with the in-plane lattice parameter of the underlying VS. Figure 1(d) shows the XRD rocking curve around the (004) Ge and (004) Si Bragg peaks together with the result of the simulation software "MadMax."[27,28] In the XRD simulation, the parabolic fit of the SIMS data, reported in Fig. 1(b), has been used as an input compositional profile. The high quality factor of the SL fringes [indicated by the red arrows in Fig. 1(d)] confirms the high crystalline quality and the regular periodicity of the PQWs in the stack. Moreover, the good agreement between XRD data and simulations confirms the parabolic symmetry of the compositional profile over a relatively large area of the sample ($\sim cm^2$).

The electronic band structure and ISBT energies of the investigated samples have been calculated self-consistently, relying on a multivalley effective mass Schrödinger–Poisson solver calibrated with material parameters obtained in detailed analysis of samples featuring similar compositions.[20,29–31] A detailed description of the model can be found in Ref. 32; here, we only mention that contributions to the Hartree potential from electrons at the Γ, Δ, and L valleys and exchange-correlation effects in the local density approximation are fully taken into account.

A parabolic well of width W and height Δ_0 (see Fig. 2) has an oscillator energy[33] $E_0 = \hbar\omega_0 = \hbar(8\Delta_0/W^2 m_z^*)^{1/2}$, where m_z^* is the effective mass in the growth direction. In our samples, $\Delta_0 \sim 120$ meV
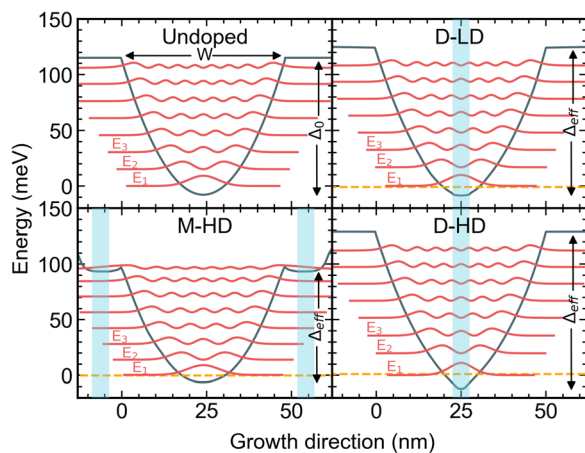
is the conduction band offset between the Ge layer at the center of the well and the $Si_{0.20}Ge_{0.80}$ barriers, $W \sim 48$–50 nm, and $m_z^* = 0.135\,m_0$. Therefore, the bare oscillator energy can be estimated as $E_0 \sim 16$ meV. However, the self-consistent confining potential is affected by the presence of both ionized donor P atoms and by electron charge distribution. Taking these effects into account, we show in Fig. 2 the L band edge profile and the squared wavefunctions, self-consistently calculated at 10 K, for samples in Table I. By comparing the bottom panels of Fig. 2, i.e., direct and modulation doping, we note that electrostatic (Hartree) charge effects influence the L band profile in a different way for the two doping geometries. As a matter of fact, when donors are introduced directly in the well, the bottom of the parabola deepens (the effective confining height Δ_{eff} increases, $\Delta_{eff} > \Delta_0$) and, for high doping, the parabolic potential is lost; consequently, the subband energies are no more equally spaced, but low energies states have a larger energy separation with respect to the bare value ($E_{12} > \hbar\omega_0$). On the contrary, in the case of modulation doping, Δ_{eff} decreases ($\Delta_{eff} < \Delta_0$). Therefore, in the case of direct doping, the Hartree potential is expected to blueshift the absorption resonance while, for the modulation doping approach, to redshift it. This is consistent with the fact that only in modulation-doped samples the depolarization blueshift can compensate for the Hartree potential, regardless of the electron density and its distribution in the subbands, and thus, Kohn theorem holds.[11,19] For the doping level investigated here, the Fermi level at 10 K lies in the fundamental subband. Therefore, all electrons occupy the fundamental subband at 10 K, but more than 60% of them are distributed in the excited subbands at room temperature.

Having discussed the electronic ISB features of our PQW samples, we now show absorption measurements performed between 10 and 300 K to investigate the dependence of the absorption resonance on doping and temperature. Absorption spectra were measured in the side-illuminated single-pass waveguide configuration with a FTIR spectrometer (Bruker Vertex 70v), equipped with a He-flow cryostat. The samples were cut and polished in a prism-waveguide geometry to couple the incoming radiation to the ISB dipole moment (i.e., TM polarized).[34,35] The dichroic transmittance $T(E)$, shown in Figs. 3(a)–3(c), is obtained as the ratio between the transmitted beam intensity in the TM and in the TE polarization. The dips at 18 (4.3), 29.5 (7.1), and 19 (4.8) meV (THz) observed at 10 K are the signatures of the intersubband transition E_{12} in samples D-LD, D-HD, and M-HD, respectively (see the supplementary material for the absorption spectrum of a reference undoped sample). The FWHM of the resonance is 6.4, 16.4, and 7.2 meV, respectively, similar to previous reports for square QWs with similar doping levels.[24,36]

Interestingly, in sample M-HD the peak energy and width are independent of temperature and close to the theoretical bare value $\hbar\omega_0$ despite the fact that, while at 10 K only the ground subband is occupied, several subbands are populated and several ISB transitions contribute to the absorption at room temperature as shown in Figs. 3(d) and 3(e), respectively. A different behavior is observed in direct doping samples. While the ISBT absorption energy of sample D-LD is only slightly redshifted by about 1 meV at high temperature, a much larger redshift is present in the D-HD sample. Furthermore, the transmittance dip of the latter sample broadens and becomes asymmetric at high temperature, suggesting that the contribution of different transitions having different absorption energies is present, as previously observed in Ge/SiGe square QWs.[36]
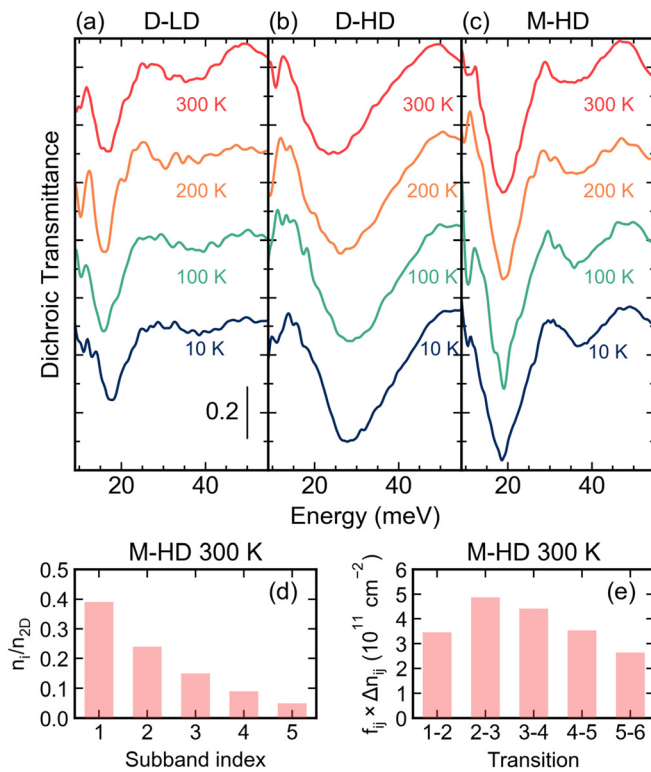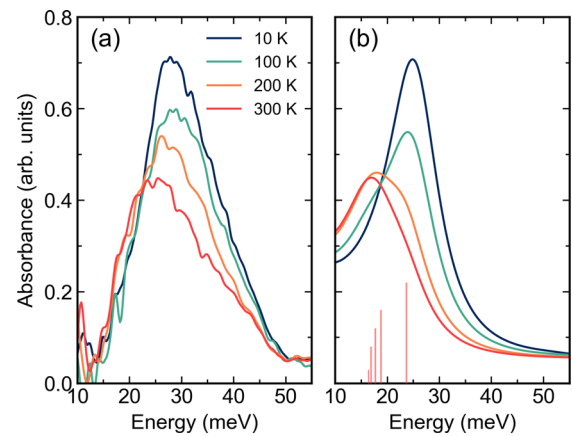

FIG. 2. Electron energies and squared wavefunctions calculated at 10 K for the samples investigated. Gray curves represent the L band profiles, while the orange dashed line corresponds to the Fermi level. The doped region in both the samples is indicated by the light blue shadows.

FIG. 3. (a)–(c) Dichroic transmittance at T = 10, 100, 200, and 300 K. Spectra are vertically shifted for clarity. Dips at $\simeq 18$ (sample D-LD), $\simeq 30$ (sample D-HD), and $\simeq 20$ meV (sample M-HD) are the signatures of the intersubband transitions. The fringes at high energy are due to interference among multiple reflections of the beam in the waveguide cavity (see Fig. S1 in the supplementary material). The electron sheet density fraction in the subbands and the spectral weight of the different ISB transitions at 300 K calculated for the M-HD sample are reported in panels (d) and (e), respectively.

FIG. 4. Measured (left panel) and calculated (right panel) α_{2D} absorbance spectra acquired on sample D-HD at different temperature values. Absorption resonances have been broadened in the simulated spectra using a Lorentzian line shape with a fixed, temperature-independent width set to the measured value at 10 K. The red vertical lines reported in panel (b) are proportional to the spectral weights of the first five transitions (from higher to lower energy: 1–2 to 5–6) contributing to the optical absorption spectrum at 300 K.

In order to confirm this hypothesis, in Fig. 4, we compare the measured and calculated α_{2D} absorbance of the D-HD sample. The simulated spectra well reproduce the behavior as a function of temperature observed experimentally. At 10 K, our simulations estimate an energy separation between the ground and the first-excited subband E_{12} larger than the bare value $\hbar\omega_0$, as shown in Fig. 2, and a 6 meV depolarization shift of the 1–2 ISB resonance [Fig. 4(b)]. As in sample M-HD, also in this case at 300 K a significant fraction of electrons occupy the excited subbands and the contribution to the absorption spectrum of transitions between excited subbands becomes dominant. However, as shown in Fig. 4(b), in sample D-HD, their absorption resonances occur at energies lower than the 1–2 absorption at 10 K because of the smaller energy separation between the excited subbands with respect to the E_{12} energy separation and the negligible depolarization shift. This explains the asymmetric and broadened line shape observed at room temperature. The comparison of the absorption spectra of samples D-LD and D-HD indicates that, to achieve a temperature-independent absorption in direct doped PQWs, the electron density must be $\sim 1 \times 10^{11}$ cm^{-2}. In this doping range, in fact, the impact of the Hartree potential and the depolarization shift on the absorption energies is < 1 meV, as estimated by our calculations.

The most relevant feature of our absorption experiment is that in modulation doped samples the absorption spectrum is independent of both temperature and subband occupation, also at much higher doping (sample M-HD) and, thus, for Hartree and many body corrections on the order of several meV. As already observed, this behavior is related to the compensation predicted by the generalized Kohn theorem of the different electron–electron interaction correction terms. The stability of the ISB absorption can also be derived in the framework of the dipole gauge Hamiltonian, considering the collective "multisubband" plasmon modes that arise from the interaction between different ISB transitions. In the work of Delteil et al.,[19] it was theoretically predicted that the ISB absorption strength in PQWs is concentrated in a single mode at the frequency of the bare ISB transition of the undoped well regardless of doping and temperature, consistent with what we experimentally observe.

Recently,[11] Al$_x$Ga$_{1-x}$As continuously graded PQWs have been grown by MBE and THz ISB transitions have been investigated as a function of temperature and doping. As in our case, the absorption energy was found to be independent of temperature, while a broadening of the absorption peak was observed at increasing temperature. For a sheet density of $n_{2D} = 3 \times 10^{11}$ cm^{-2}, thus slightly smaller than that in sample M-HD, the authors reported that $\Delta E/E$ raised from 12% to 30% when the temperature was increased from 77 K to room temperature. In sample M-HD, we found $\Delta E/E \sim 35\%$, independent of temperature. Thus, at room temperature, the $\Delta E/E$ values are comparable for the two material systems.

In conclusion, we have demonstrated the growth of high-quality, continuously graded Si$_{1-x}$Ge$_x$ PQWs by UHV-CVD. Well-defined ISB absorption features are clearly observed up to 300 K. Modulation doped samples feature a sharp ISB absorption peak whose energy position and shape do not change upon increasing the lattice temperature from 10 K up to 300 K, also in the high doping regime. Remarkably, the spectral width is comparable to the one observed at room temperature in similar PQW samples based on III–V compounds. These

achievements demonstrate that the improvements made in the epitaxy of Ge-rich SiGe heterostructures on Si substrates make this material platform competitive with respect to the III–V semiconductor one and represent a relevant step forward toward the development of THz devices compatible with the CMOS technology.

See the supplementary material for the dichroic transmittance of a reference undoped sample.

DATA AVAILABILITY

The data that support the findings of this study are available from the corresponding author upon reasonable request.

REFERENCES

[1]J. Faist, F. Capasso, D. L. Sivco, C. Sirtori, A. L. Hutchinson, and A. Y. Cho, Science **264**, 553 (1994).
[2]M. S. Vitiello, G. Scalari, B. Williams, and P. D. Natale, Opt. Express **23**, 5167 (2015).
[3]J. Faist, *Quantum Cascade Lasers* (Oxford University Press, 2013).
[4]H. Schneider, *Quantum Well Infrared Photodetectors—Physics and Applications*, 1st ed., Springer Series in Optical Sciences (Springer, 2006).
[5]D. Palaferri, Y. Todorov, Y. N. Chen, J. Madeo, A. Vasanelli, L. H. Li, A. G. Davies, E. H. Linfield, and C. Sirtori, Appl. Phys. Lett. **106**, 161102 (2015).
[6]P. Jouy, A. Vasanelli, Y. Todorov, L. Sapienza, R. Colombelli, U. Gennser, and C. Sirtori, Phys. Rev. B **82**, 045322 (2010).
[7]P.-B. Vigneron, S. Pirotta, I. Carusotto, N.-L. Tran, G. Biasiol, J.-M. Manceau, A. Bousseksou, and R. Colombelli, Appl. Phys. Lett. **114**, 131104 (2019).
[8]Y. Todorov, A. M. Andrews, R. Colombelli, S. De Liberato, C. Ciuti, P. Klang, G. Strasser, and C. Sirtori, Phys. Rev. Lett. **105**, 196402 (2010).
[9]J. Ulrich, R. Zobl, K. Unterrainer, G. Strasser, E. Gornik, K. D. Maranowski, and A. C. Gossard, Appl. Phys. Lett. **74**, 3158 (1999).
[10]M. Geiser, F. Castellano, G. Scalari, M. Beck, L. Nevou, and J. Faist, Phys. Rev. Lett. **108**, 106402 (2012).
[11]C. Deimert, P. Goulain, J.-M. Manceau, W. Pasek, T. Yoon, A. Bousseksou, N. Y. Kim, R. Colombelli, and Z. R. Wasilewski, Phys. Rev. Lett. **125**, 097403 (2020).
[12]W. Kohn, Phys. Rev. **123**, 1242 (1961).
[13]L. Brey, N. F. Johnson, and B. I. Halperin, Phys. Rev. B **40**, 10647 (1989).
[14]K. Isensee, N. Kröger-Lui, and W. Petrich, Analyst **143**, 5888 (2018).
[15]M. Geiser, G. Scalari, F. Castellano, M. Beck, and J. Faist, Appl. Phys. Lett. **101**, 141118 (2012).
[16]K. D. Maranowski and A. C. Gossard, J. Appl. Phys. **88**, 172 (2000).
[17]R. C. Miller, A. C. Gossard, D. A. Kleinman, and O. Munteanu, Phys. Rev. B **29**, 3740 (1984).
[18]C. Deimert and Z. Wasilewski, J. Cryst. Growth **514**, 103 (2019).
[19]A. Delteil, A. Vasanelli, Y. Todorov, C. Feuillet Palma, M. Renaudat St-Jean, G. Beaudoin, I. Sagnes, and C. Sirtori, Phys. Rev. Lett. **109**, 246808 (2012).
[20]C. Ciano, M. Virgilio, M. Montanari, L. Persichetti, L. Di Gaspare, M. Ortolani, L. Baldassarre, M. Zoellner, O. Skibitzki, G. Scalari, J. Faist, D. Paul, M. Scuderi, G. Nicotra, T. Grange, S. Birner, G. Capellini, and S. M. De, Phys. Rev. Appl. **11**, 014003 (2019).
[21]G. Capellini, M. De Seta, Y. Busby, M. Pea, F. Evangelisti, G. Nicotra, C. Spinella, M. Nardone, and C. Ferrari, J. Appl. Phys. **107**, 063504 (2010).
[22]A. Ballabio, J. Frigerio, S. Firoozabadi, D. Chrastina, A. Beyer, K. Volz, and G. Isella, J. Phys. D: Appl. Phys. **52**, 415105 (2019).
[23]O. Skibitzki, M. H. Zoellner, F. Rovaris, M. A. Schubert, Y. Yamamoto, L. Persichetti, L. Di Gaspare, M. De Seta, R. Gatti, F. Montalenti, and G. Capellini, Phys. Rev. Mater. **4**, 103403 (2020).
[24]M. Virgilio, D. Sabbagh, M. Ortolani, L. Di Gaspare, G. Capellini, and M. De Seta, Phys. Rev. B **90**, 155420 (2014).
[25]G. Capellini, M. De Seta, P. Zaumseil, G. Kozlowski, and T. Schroeder, J. Appl. Phys. **111**, 073518 (2012).
[26]C. Manganelli, M. Virgilio, O. Skibitzki, M. Salvalaglio, D. Spirito, P. Zaumseil, Y. Yamamoto, M. Montanari, W. Klesse, and G. Capellini, J. Raman Spectrosc. **51**, 989 (2020).
[27]O. Brandt, P. Waltereit, M. Kastner, and D. Schaadt, "MadMax-Massively accelerated dynamical multilayer analysis by x-ray diffraction," 2001-2005.
[28]O. Brandt, P. Waltereit, and K. H. Ploog, J. Phys. D: Appl. Phys. **35**, 577 (2002).
[29]M. Montanari, M. Virgilio, C. L. Manganelli, P. Zaumseil, M. H. Zoellner, Y. Hou, M. A. Schubert, L. Persichetti, L. Di Gaspare, M. De Seta, E. Vitiello, E. Bonera, F. Pezzoli, and G. Capellini, Phys. Rev. B **98**, 195310 (2018).
[30]L. Persichetti, M. Montanari, C. Ciano, L. Di Gaspare, M. Ortolani, L. Baldassarre, M. Zoellner, S. Mukherjee, O. Moutanabbir, G. Capellini, M. Virgilio, and M. De Seta, Crystals **10**, 179 (2020).
[31]C. Ciano, L. Persichetti, M. Montanari, L. Di Gaspare, G. Capellini, L. Baldassarre, M. Ortolani, A. Pashkin, M. Helm, S. Winnerl, M. Virgilio, and M. De Seta, Phys. Rev. B **102**, 205302 (2020).
[32]L. Bagolini, M. Montanari, L. Persichetti, L. Di Gaspare, G. Capellini, M. Ortolani, M. D. Seta, and M. Virgilio, Phys. Rev. B **101**, 245302 (2020).
[33]K. D. Maranowski, A. C. Gossard, K. Unterrainer, and E. Gornik, Appl. Phys. Lett. **69**, 3522 (1996).
[34]M. De Seta, G. Capellini, Y. Busby, F. Evangelisti, M. Ortolani, M. Virgilio, G. Grosso, G. Pizzi, A. Nucara, and S. Lupi, Appl. Phys. Lett. **95**, 051918 (2009).
[35]Y. Busby, M. De Seta, G. Capellini, F. Evangelisti, M. Ortolani, M. Virgilio, G. Grosso, G. Pizzi, P. Calvani, S. Lupi, M. Nardone, G. Nicotra, and C. Spinella, Phys. Rev. B **82**, 205317 (2010).
[36]M. D. Seta, G. Capellini, M. Ortolani, M. Virgilio, G. Grosso, G. Nicotra, and P. Zaumseil, Nanotechnology **23**, 465708 (2012).